This document was prepared for the ETI by third parties under contract to the ETI. The ETI is making these documents and data available to the public to inform the debate on low carbon energy innovation and deployment.

Programme Area: Marine

Project: PerAWAT

Title: Verification of Code

Abstract:

This deliverable investigates coastal basin scale modelling of tidal energy extraction. The aim of the work package is to extract a robust methodology for evaluating the power extracted, and the change to tidal dynamics caused by inserting turbines into a tidal basin. This report presents a verification of the numerical ADCIRC code which is to be used in this work package. Various test cases have been run and agreement has been found with relevant analytical, numerical and experimental results. The code has been applied to an actual tidal inlet using measured bathymetry and coast line tidal forcing extracted from a database.

Context:

The Performance Assessment of Wave and Tidal Array Systems (PerAWaT) project, launched in October 2009 with £8m of ETI investment. The project delivered validated, commercial software tools capable of significantly reducing the levels of uncertainty associated with predicting the energy yield of major wave and tidal stream energy arrays. It also produced information that will help reduce commercial risk of future large scale wave and tidal array developments.

Energy Technologies Institute

PerAWaT

WG3 WP6 D2: VERIFICATION OF CODE

Authors T.A.A. Adcock, S. Serhadlioglu,
G.T. Houlsby, and A.G.L. Borthwick

Version 2.0

Date 24 June 2011

Revision History		
Issue / Version	Issue Date	Summary
0.1	2/5/2011	For internal/GLGH review
1.0	17/5/2011	Submitted to ETI
2.0	24/6/2011	Revisions in response to reviewers comments

Executive summary

This deliverable presents a verification of the numerical ADCIRC DG code which is to be used for this work package. Various test cases have been run and agreement has been found with relevant analytical, numerical or experimental results.

Due to the choice of code, no code adaptation has been required to apply DG ADCIRC to a real location. To demonstrate this, the code has been applied to an actual tidal inlet using measured bathymetry and coastline and tidal forcing extracted from a database.

A discussion is presented of the applications, limitations and sensitivities of the modelling undertaken as part of this work package.

Table of contents

1. Introduction

WG3 WP6 investigates the basin scale modelling of tidal energy extraction. The aim of the work package is to establish a robust methodology for evaluating the power extracted, and the change to the tidal dynamics, caused by inserting turbines into a tidal basin.

The work package will look at three different locations around the United Kingdom where there are fast flowing tidal streams. The rationale for choosing these sites will be given in WG3 WP6 D3. The sites chosen are the Pentland Firth (a strait/headland), Anglesey (headland) and the Bristol Channel (estuary). This complements the work being carried out by EDF in WG3 WP3. All the sites selected are shown in Figure 1, along with those being studied by EDF.

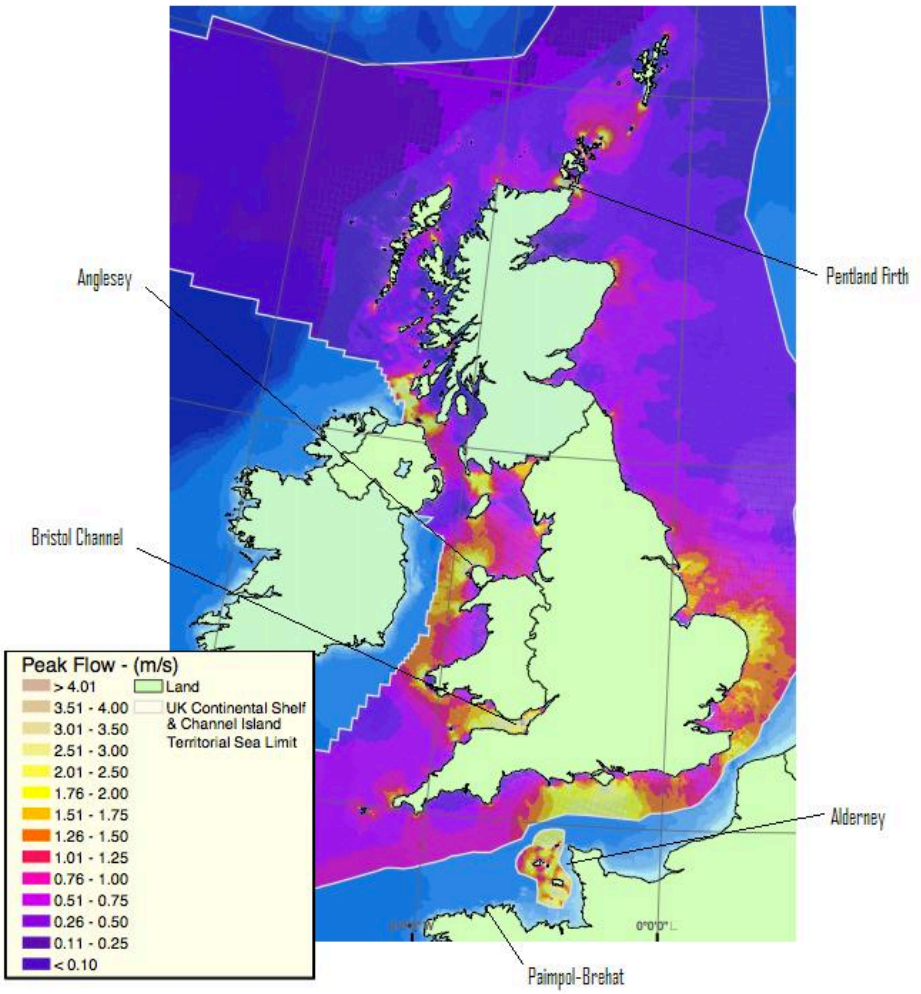

Figure 1 Map of the UK showing the sites. Contours show peak spring current (UK waters only). Taken from DTI atlas

The methodology for this work package is as follows. A numerical model will be developed to simulate the naturally occurring tidal dynamics. The model will be validated against field measurements and, if available, other models. Turbines will then been inserted into the numerical model as a line discontinuity, using linear momentum actuator disc theory (see Draper et al., 2010). The power produced by the turbines may then be investigated as well as the changes to the naturally occurring tidal dynamics.

The numerical model to be used is the discontinuous Galerkin version of ADCIRC (Kubatko et al, 2006). The rationale for this choice is given in WG3 WP6 D1. In this deliverable we present verification of the code for various benchmark tests and demonstration that the code may be applied to real sites. We also present a review of the applications, sensitivities and limitations of the numerical model.

Due to the choice of code, no major adaptation of the code has been required as part of this deliverable. Small changes were needed as part of the verification tests so that the relevant initial condition, or boundary condition, could be modelled in respectively the Coriolis test case and the eddy viscosity test. These edits were carried out on an *ad hoc* basis and do not alter the code used for the modelling of real locations. The DG ADCIRC code is well documented in literature and has been widely applied in practice. We do not repeat previous reported verification and validation tests in this report. However, the verification tests required for the present deliverable have not previously been implemented or reported. We demonstrate that the code may be applied to a realistic location by modelling an actual tidal inlet.

A key limitation and sensitivity of this work is the location of the offshore boundary and the size of the domain to be modelled. We have analysed this problem in detail, the results of which have been submitted to EWTEC 2011 (Adcock et al., 2011). This paper is included as an appendix to this report.

Acceptance criteria

The acceptance criteria for this deliverable are detailed in the table below, along with the sections of this report which fulfill these.

Description of methodology for code adaption including all algorithms and assumptions	Due to the choice of code no code adaptation has been required. This is demonstrated in section 3.
Evidence of functional validation against numerical benchmark tests covering each of: bathymetry, bed shear, horizontal eddy viscosity, Coriolis forces and tidal energy extraction.	These tests are carried out in section 2.
Assessment of model performance based on validation exercises – including review of applications, sensitivities and limitations.	These are set out in sections 4 to 6.

Table 1 Deliverable acceptance criteria.

2. Verification tests

The strategy used in the verification tests is to examine each term, one at a time, in the shallow water equations. Thus tests are used where parameters not being directly tested are set to zero (if possible). Finally, we demonstrate the application of the code to the hydrodynamics of a real tidal inlet.

Bed friction

This verification test examines the ability of the numerical solver to handle the bed slope and bed shear stress terms in the shallow water equations. The test consists of a rectangular channel, which has the dimensions of $(x,y)\in[0,1000]\times[0,400]$ m, with a constant slope of 0.001. The water depth throughout the channel is 5 m. The numerical mesh consists of 320 structured elements and has a spatial resolution of 50 m (Figure 2). The time step is set to 0.5 s, a value that satisfies the Courant–Friedrichs–Lewy (CFL) condition. On the lateral walls, slip boundary conditions are applied. The free surface elevation is

prescribed by constant values at the upstream and downstream boundaries and initially is set to vary linearly (i.e. have constant depth) between the end boundaries. In this test, the kinematic eddy viscosity, Coriolis force, and wind stresses are all ignored. Using a quadratic bed friction coefficient of C_f = 0.005, an analytical value of depth-averaged velocity can be calculated (Wijbenga, 1985),

$$u = \sqrt{\frac{gRS_0}{C_f}}, \qquad 1$$

which is obtained by balancing the water weight component along the inclined channel to the bed resistance. In Equation (1) g is the acceleration due to gravity, R is the hydraulic radius that can be taken as the water depth (for a wide channel), and S_o is the bed slope. The theoretical velocity is calculated as 3.132091952673 m/s. The numerical model reached equilibrium at a flow simulation time t = 2880 s, and predicted a steady state value of 3.13209195267285 m/s to 12 significant figures (Figure 2). The excellent agreement between the numerical and analytical predictions indicates that the discontinuous Galerkin ADCIRC model is capable of modelling flows in an inclined channel with bed shear stress and that these terms are correctly implemented in the code.

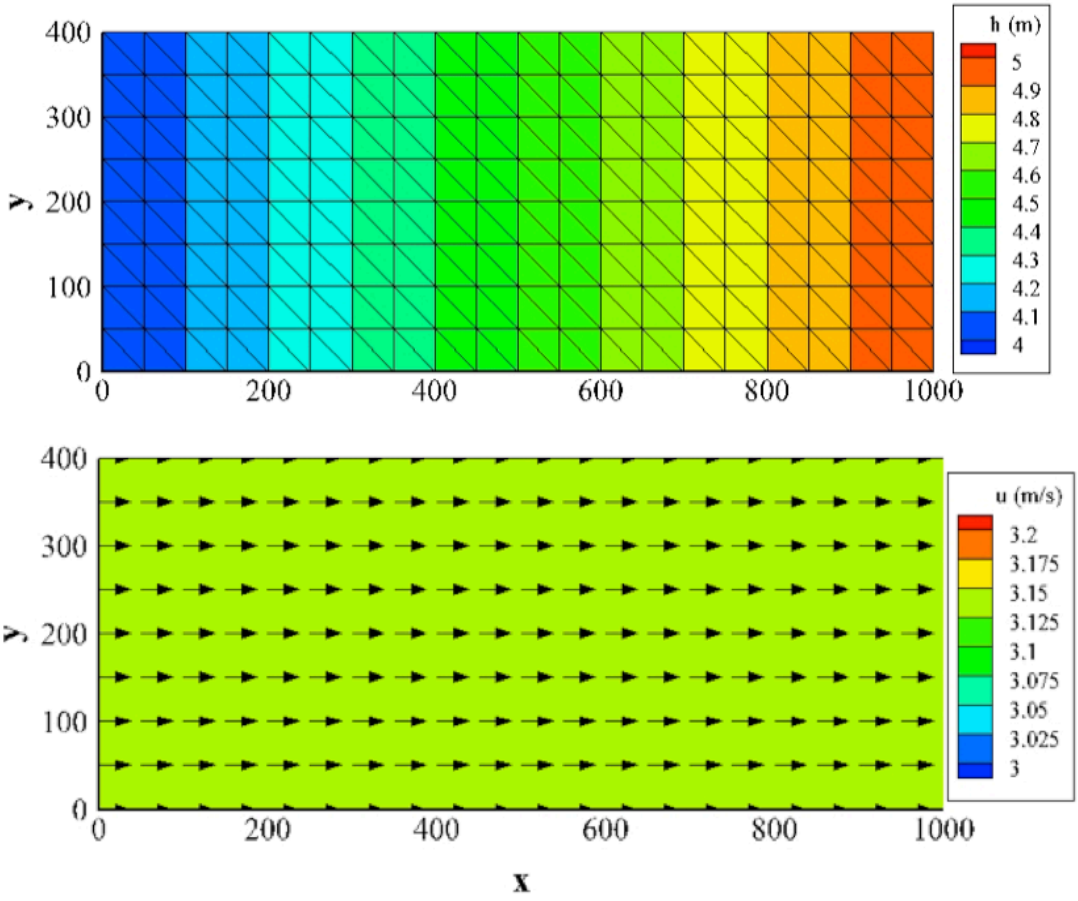

Figure 2 Bed friction test. x and y axes are in m. Above: bathymetry. Lower: velocity contours and vector

Eddy viscosity

Two-dimensional laminar flow through an idealized rectangular channel with a sudden side-wall expansion provides a test as to how well the model reproduces viscous flow separation. Free surface flow in an open channel with a sudden width expansion, is analogous to flow over a backward facing step, which has been a subject of several papers in the hydraulics literature. At steady state, the flow separates at the expansion in the width of the channel and forms a recirculation zone downstream. Experimental data from Denham and Patrick (1974) and O'Leary and Mueller (1969) show that for laminar flow, the length of the recirculation zone is dependent on the upstream Reynolds number (*Re*). However, for upstream Reynolds numbers greater than 2000, O'Leary and Meuller (1969) find that the recirculation length is independent of the Reynolds number.

The Reynolds number is defined as,

$$Re = \frac{U_c L_c}{\upsilon}, \qquad 2$$

in which U_c is a characteristic velocity, L_c is a characteristic length, and υ is the kinematic eddy viscosity coefficient. In the literature, the Reynolds number has been defined in at least two ways in terms of the domain dimensions. Denham and Patrick (1974) use the form

$$Re = \frac{U_{inlet} h}{\upsilon}, \qquad 3$$

where U_{inlet} is the average upstream velocity across the inlet section, h is the step-size (half the distance across the upstream channel). However, Armaly et al. (1983) take the characteristic length scale to be $2h$, the distance across the upstream channel (which represents the hydraulic diameter of the upstream channel). In the present work, the approach used by Denham and Patrick (1974) is adopted.

Assuming that free surface effects are small, it is reasonable to compare the results obtained by Denham and Patrick (1974) with the numerical predictions obtained using the discontinuous Galerkin ADCIRC model. The comparison between the reattachment lengths obtained by both the present numerical simulation and Denham and Patrick's experiment is then used to confirm that the numerical scheme is capable of reproducing viscous flow effects correctly.

The computational domain geometry used in this validation test is same as adopted by Denham and Patrick (1974), which can be seen in Figure 3.

The flow is forced using a fully developed parabolic velocity profile at the inlet boundary, the analytical solution for Poiseuille flow (Schlichting, 1968). In this case, the inlet flow velocity profile is,

$$U(y) = \frac{3}{2} U_{inlet} \left(1 - \left(\frac{y-h}{h}\right)^2\right), \qquad 4$$

In the numerical model, h = 1.0 m. A ramping function is used to prevent shocks in the computation. The test is run for a elements which have a polynomial order

of $n = 3$. The computational mesh has a resolution of 0.25 m with 2304 structured elements.

The streamlines shown in Figure 4 are created using Tecplot post-processor. It can be seen that the reattachment length varies with respect to the inlet Reynolds number. A comparison of the reattachment lengths is shown in Figure 5 where the results of the DG ADCIRC code are compared to both experimental data and the results of the Oxtide DG shallow water code (Draper, 2011). This comparison shows good agreement between the two numerical codes. For large Reynolds numbers there is a significant discrepancy between the experimental and numerical results. One cause of this discrepancy can be seen in Figure 6 where we compare the flow profiles in the domain. It can be seen that the flow is not fully developed at the step in the experiments, as the flow is clearly not symmetric or parabolic.

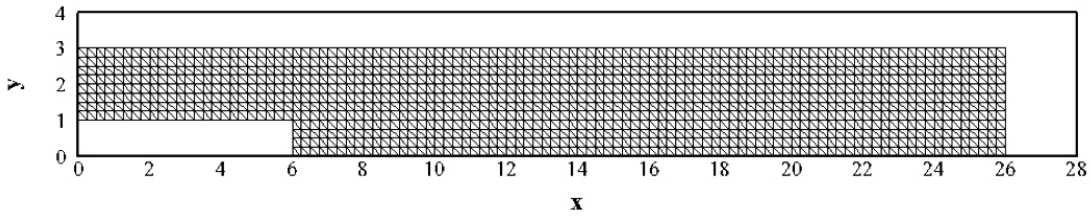

Figure 3 Eddy viscosity test. Mesh used for side wall expansion. Axes have units of meters.

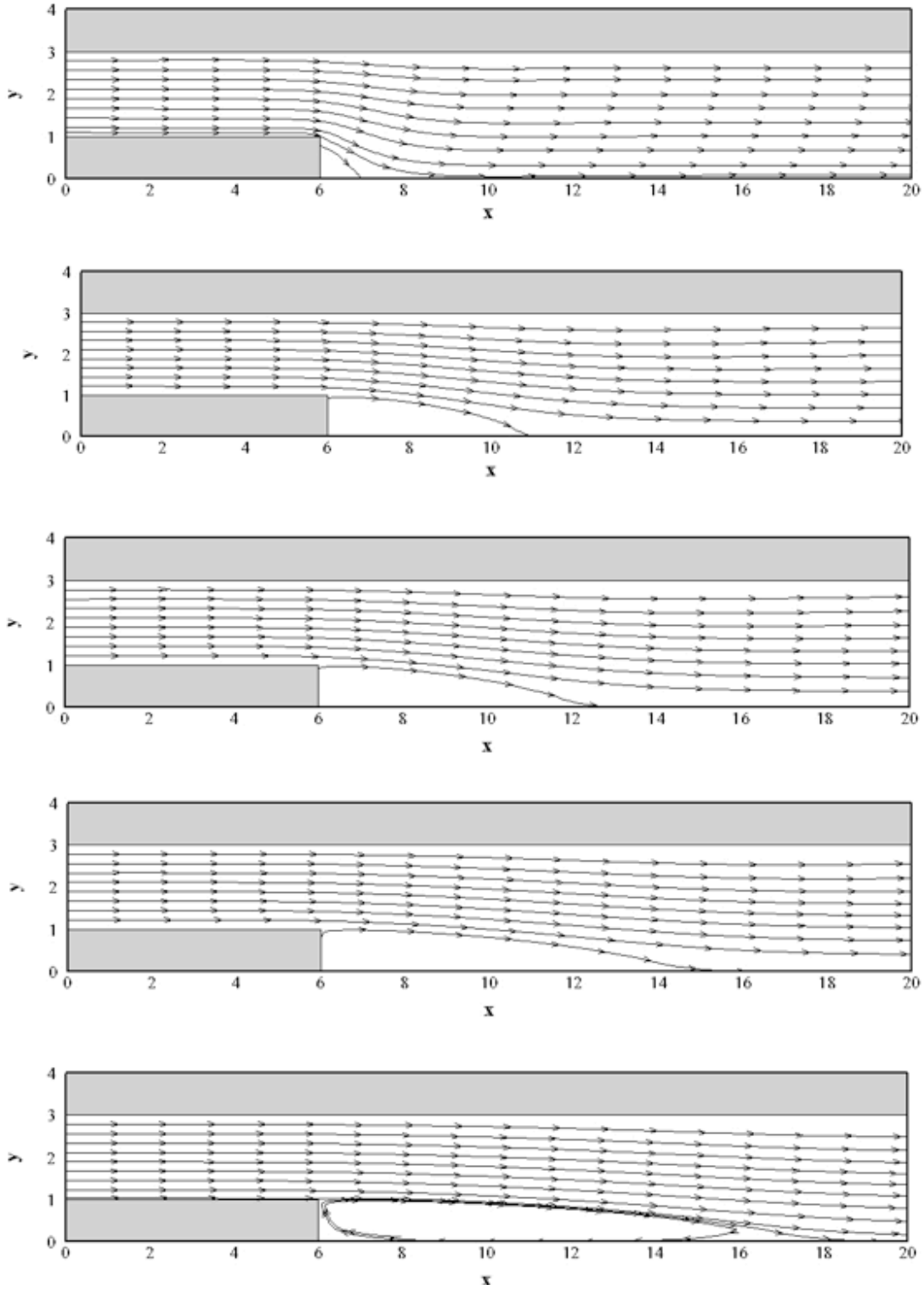

Figure 4 Eddy viscosity test. Streamlines. Axes are in meters. From top to bottom the inlet Reynolds numbers are: 7.9; 73; 98; 150; 229.

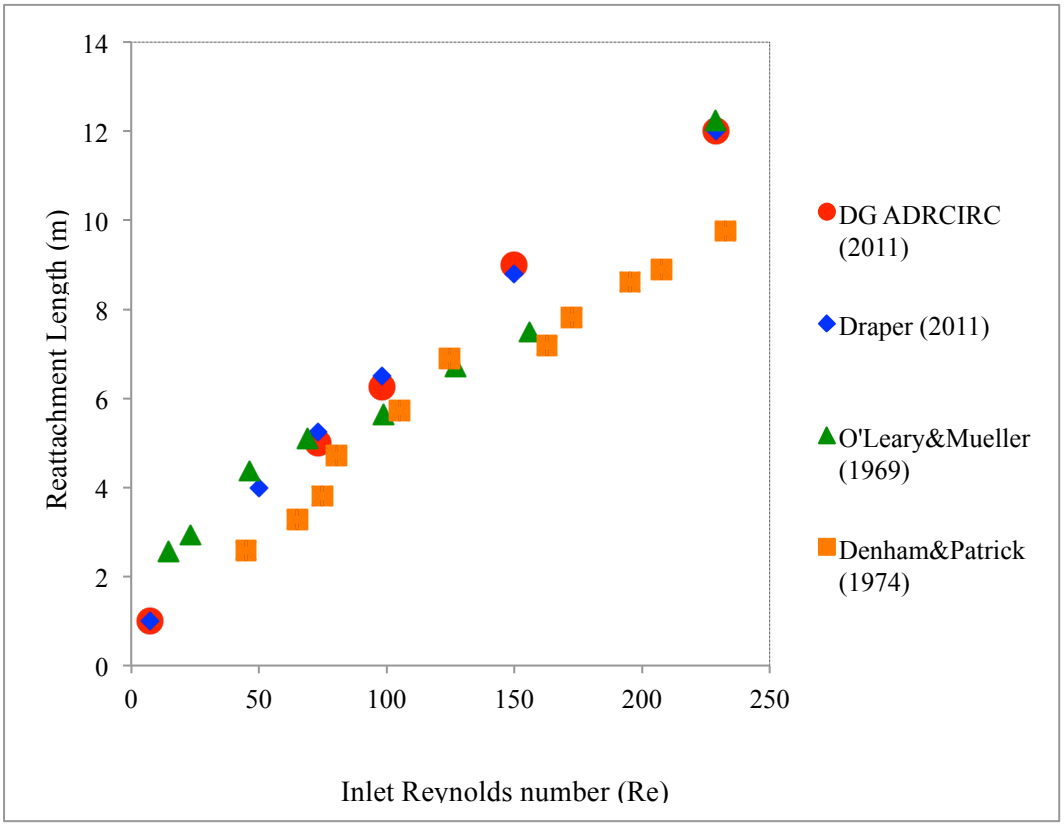

Figure 5 Comparison of reattachment length for different numerical and physical models

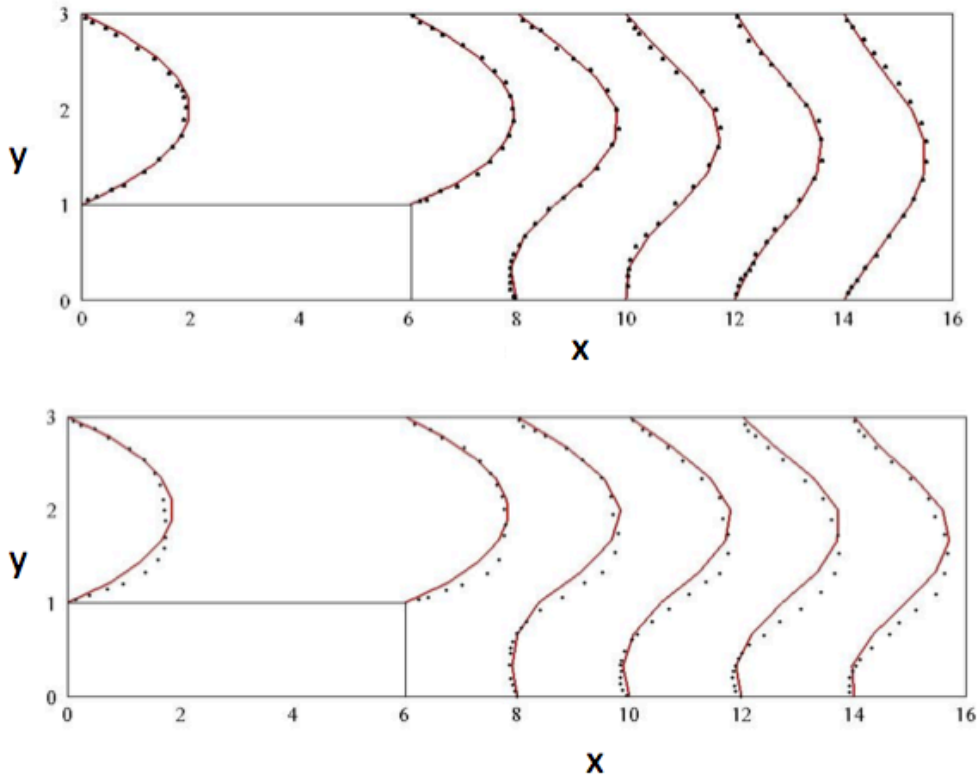

Figure 6 Velocity profiles from experimental (Denham & Patrick, 1974) dots and ADCIRC DG numerical results (line). Axes are in meters. Above *Re*=73. Below *Re*=229.

Coriolis term

To test the Coriolis source term we examine the propagation of an equatorial Kelvin wave for which an analytical solution exists. In this test the shallow water equations simplify to

$$\frac{\partial h}{\partial t}+\frac{\partial u}{\partial x}+\frac{\partial v}{\partial y}=0 \quad (5)$$

$$\frac{\partial u}{\partial t}+g\frac{\partial h}{\partial x}=fv \quad (6)$$

$$\frac{\partial u}{\partial t}+g\frac{\partial h}{\partial y}=-fu \quad (7)$$

Following Eskilsson and Sherwin (2000) and Giraldo and Warburton (2008), the system of equations given in Equations (5) to (7) is rewritten in non-dimensional form. Using primes to denote non-dimensional variables, the physical parameters can be expressed as, $x=R/E^{1/4}\,x'$, $t=E^{1/4}/2\Omega\,t'$, $h=h_o h'$, $u=(g\,h_o)^{1/2}u'$, $f=2\Omega/\,E^{1/4}y'$. E denotes the Lamb parameter, $E=4\Omega^2R^2/gh_o$, R is the radius of the Earth, Ω is the angular velocity of the Earth's rotation (i.e. 2π/day), and h_o is the mean depth, which is taken as 0.4 m. The initial conditions (Eskilsson and Sherwin, 2000) define a mound of water that should propagate westward under the influence of the Coriolis force, and are expressed as

$$h'(x,t)=\exp\left(-\frac{y'^2}{2}\right)\exp\left(-\frac{(x'+5-t')^2}{2}\right), \quad (8)$$

$$u'(x,t)=\exp\left(-\frac{y'^2}{2}\right)\exp\left(-\frac{(x'+5-t')^2}{2}\right), \quad (9)$$

$$v'(x,t)=0. \quad (10)$$

A non-dimensional computational domain is used, with 4096 structural triangular elements and third order polynomials. Using the beta-plane approximation, the Coriolis parameter is written $f=f_0+\beta y$. By setting f_0 to 0, the β parameter is obtained as $2\Omega/R$, while y is the coordinate positive northwards. Boundary conditions at the inflow and outflow boundaries are defined by

specifying the normal flux using equations (8) to (10). On the walls, a slip boundary condition is applied. The mesh resolution is $r = 0.3125$. Figure 7 shows the propagation of linear Kelvin wave. The results agree with the analytical solution as shown in Figure 8.

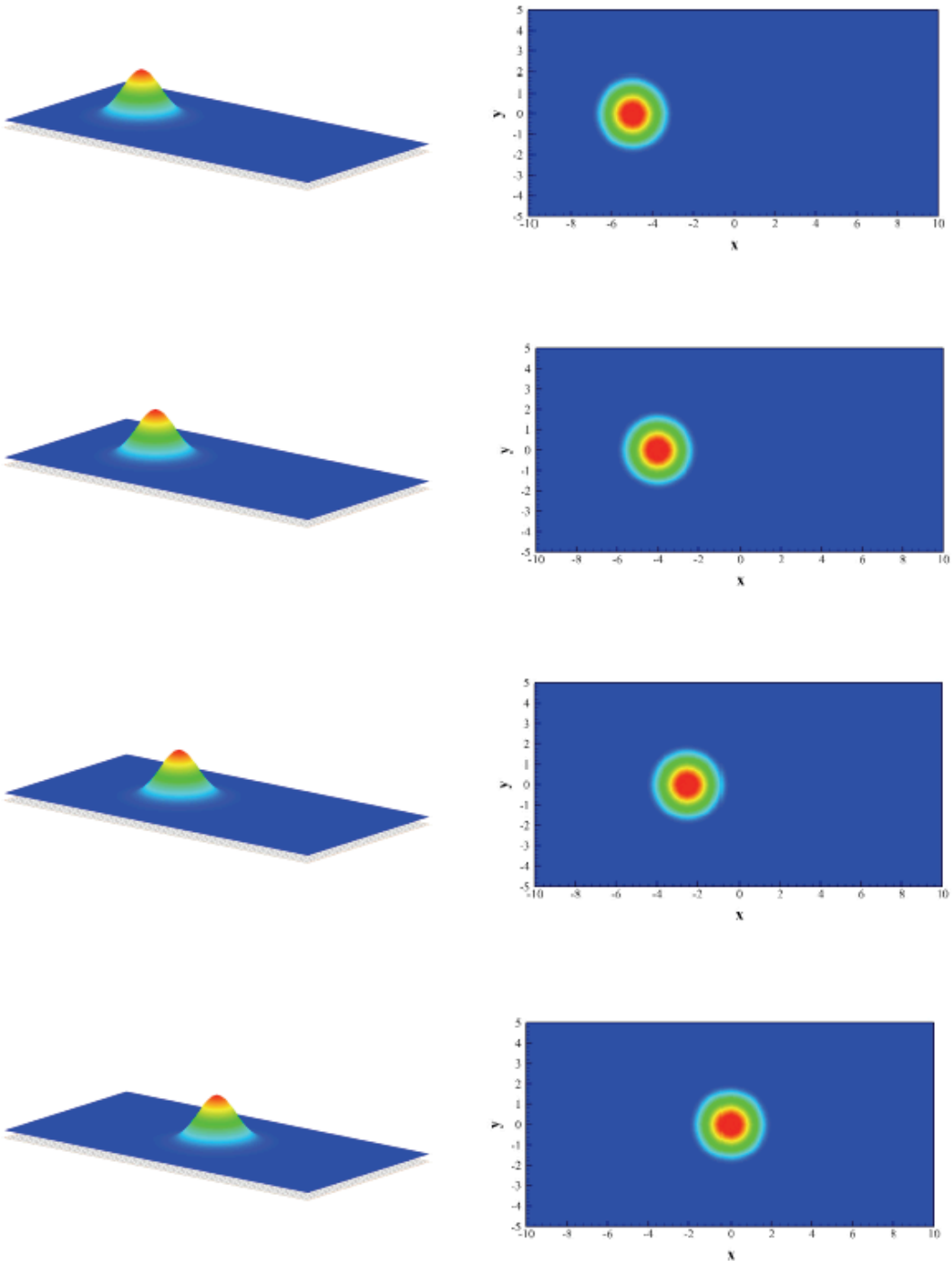

Figure 7 Coriolis test: Propagation of Kelvin wave across domain. From top to bottom t'=0, t'=1, t'=2.5, t'=5.

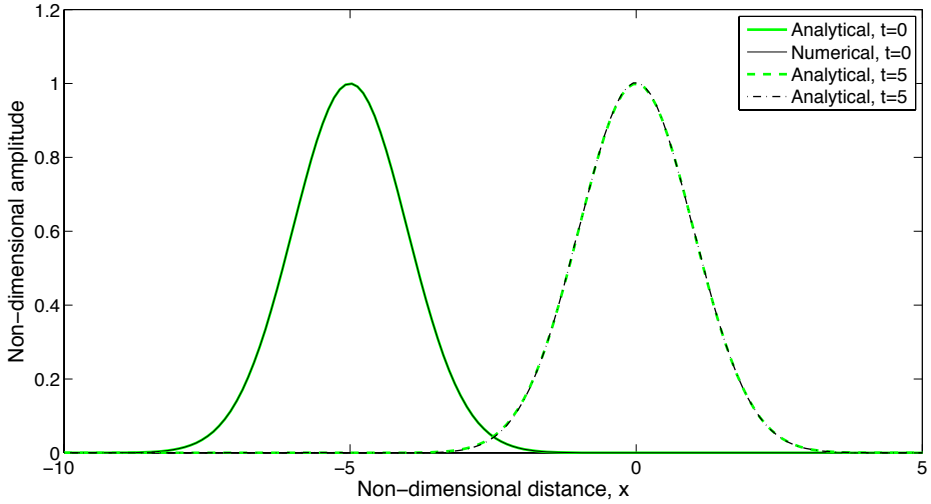

Figure 8 Coriolis test: Comparisons of analytical and numerical results at different times. Section taken through data at y=0.

Energy extraction

To test the energy extraction from the model we use a simple channel where a current is driven by a head difference. We take a channel that is 1000 m long and 500 m in width. The bed is flat. The channel is meshed as shown in Figure 9. At the ends of the channel the amplitude is held constant: at one end the depth is 4.5 m; at the other the depth is 4 m. On the side boundaries a non-slip boundary condition is applied. We apply a bed friction coefficient C_f = 0.0025.

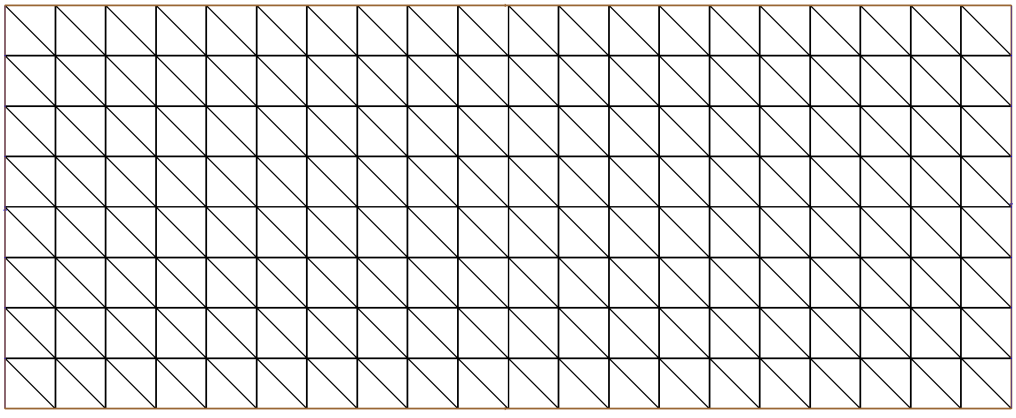

Figure 9 Mesh used for energy extraction case

We initalise the water level across the domain so that it varies linearly between the upstream and downstream boundaries. Initially the current is set to zero. After the model is started the current increases until it reaches a steady state. This is shown in Figure 10 where we plot flow rate rather than current, as this is constant across the domain.

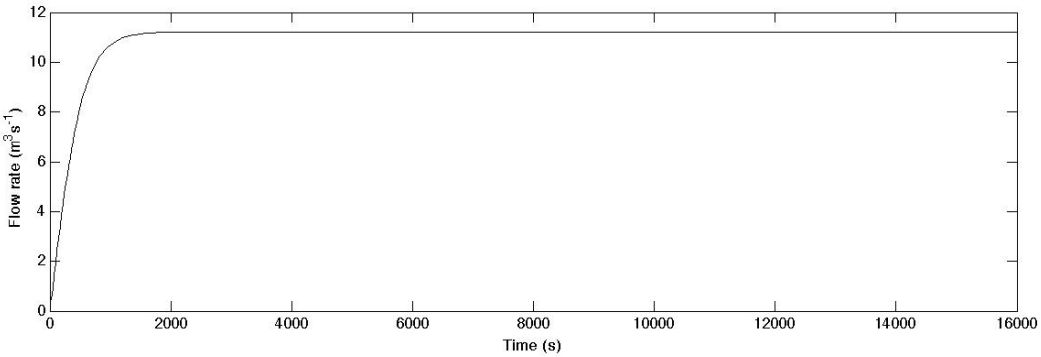

Figure 10 Energy extraction case: time variation in flow rate through channel.

We now introduce additional bed roughness, which has been used to represent the action of tidal turbines and extract energy (Sutherland et al., 2007). We add extra roughness over a width of 100 m (i.e. two cells). The extra roughness causes a reduction in the mass flow rate and an increase in the drop in the free surface across the cells with enhanced roughness. We show this in Figure 11.

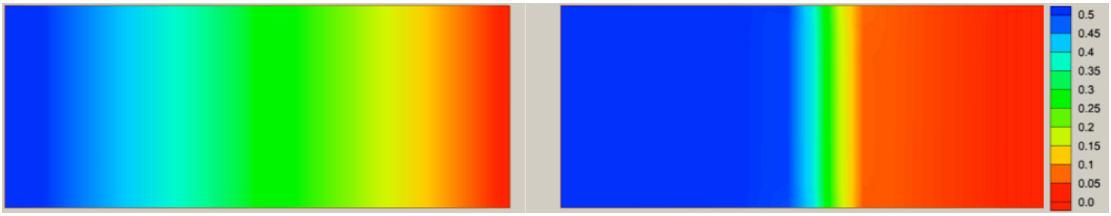

Figure 11 Free surface in energy extraction case. Left shows case with no additional roughness. Right shows the free surface for an energy extraction case.

This problem was analysed analytically by Garrett & Cummins (2005). They showed that the peak power output occurred when the flow was 58% of the undisturbed flow and that the rate of energy extracted is given by

$$\frac{P}{P_{max}} = \left(\frac{3^{\frac{3}{2}}}{2}\right)\left(\frac{Q}{Q_{max}}\right)\left[1-\left(\frac{Q}{Q_{max}}\right)^{2}\right], \qquad 11$$

where P is the power extracted and Q is the mass flow rate. The peak power is given by

$$P_{max} = \gamma \rho g a Q_{max}, \qquad 12$$

where γ is a constant equal to 0.38 for a steady state channel, ρ is the density of the fluid, a is the headloss across the channel, and Q_{max} is the undisturbed mass flow rate.

The power extracted from the flow in the numerical model is given by

$$P = \sum_{\text{Rough Area}} C_t \rho u^3, \qquad 13$$

where C_t is the drag due to the turbines. The energy extracted from the numerical model is compared to the analytical solution in Figure 12. It can be seen that there is excellent agreement between the present numerical model and the analytical solution.

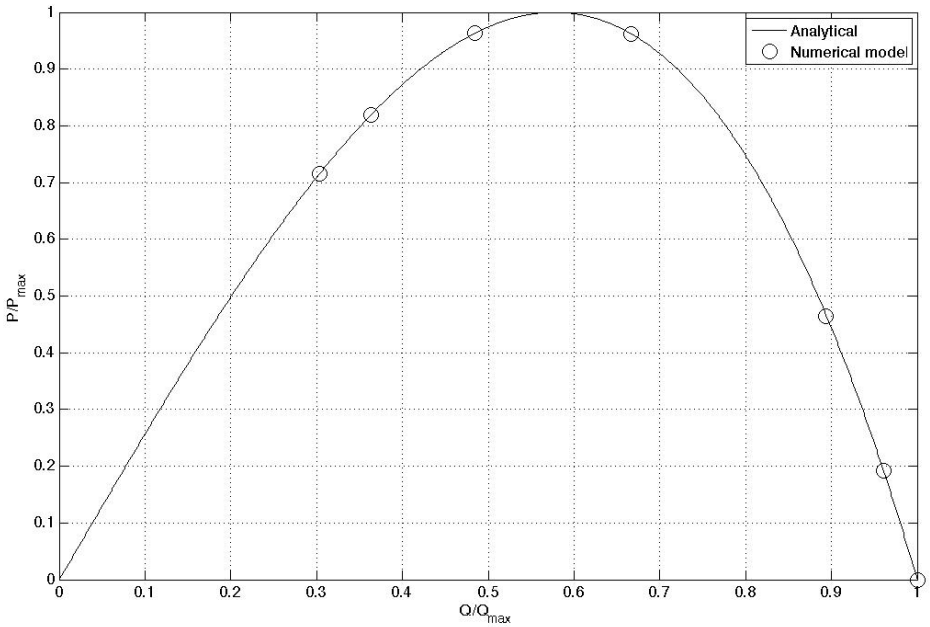

Figure 12 Extraction of power from code compared with analytical solution of Garrett & Cummins (2005)

Flux balance

In this test case, the aim is to check that the bed source terms properly balance the flux gradient terms in the numerical model. In certain applications, problems

may arise due to the irregular bed topography of the numerical domain, which may include extreme bed slopes with high bed roughness (Brufau et al., 2002). When such gradients are not handled correctly, spurious flows may appear in the solution (Bermudez and Vazques, 1994; Bunya et al., 2009). To carry out the check, the benchmark case proposed by Ern et al. (2008) is used to verify the discontinuous Galerkin ADCIRC model for still water over non-uniform bathymetry. Ern et al. (2008) considered a one-dimensional domain, whose bed is given by equation (14) and shown in Figure 13. Initially the water level is set to 1 m above a fixed horizontal datum and the flow velocity set to zero throughout the domain. The grid resolution is 1m and a second order polynomial is used. The bed profile is

$$b(x) = \frac{10e^{-x^2} + 15e^{-(x-2.5)^2} + 10e^{\frac{-(x-5)^2}{2}} + 6e^{-2(x-7.5)^2} + 16e^{-(x-10)^2}}{20}. \qquad 14$$

The two-dimensional grid is shown in Figure 13. The model is run for 25 minutes of simulation time. Still water level is maintained as shown in Figure 14. The still water level remains exactly consistent throughout the simulation.

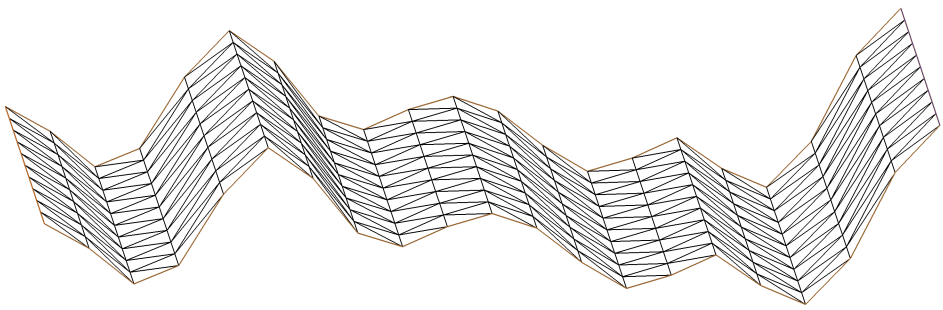

Figure 13 Bed profile and mesh used in still water test

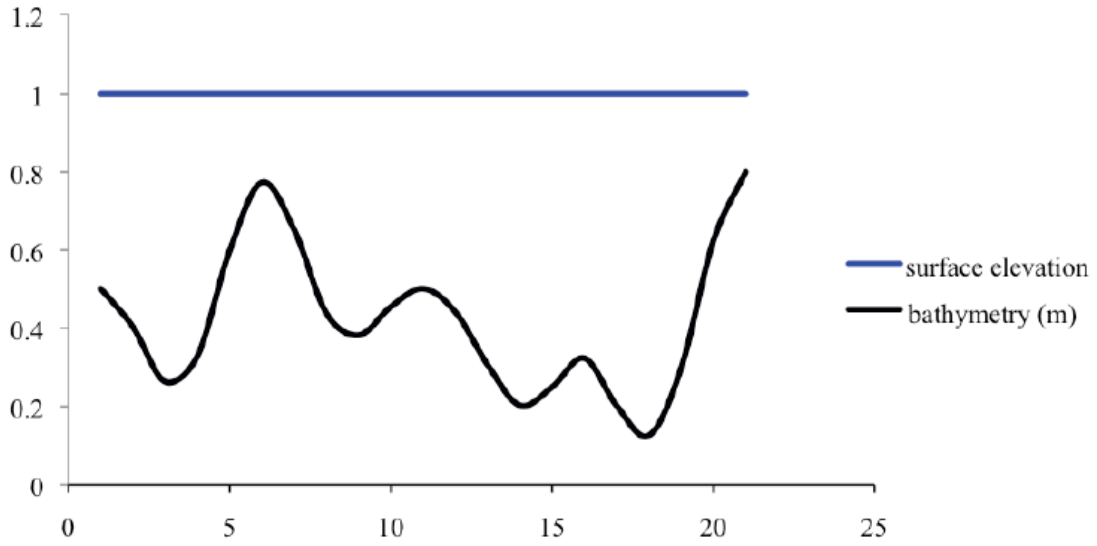

Figure 14 Still water test: free surface elevation after 25 minutes. Axes are in m

3. Application of DG ADCIRC to a real location

In this section we demonstrate that the code may be applied to a complicated actual geometry with realistic boundary conditions. We consider Shinnecock Bay and Inlet off the coast of Long Island, New York State. This location has been studied using CG ADCIRC (Militello & Zundel, 2002). This location is shown in Figure 15.

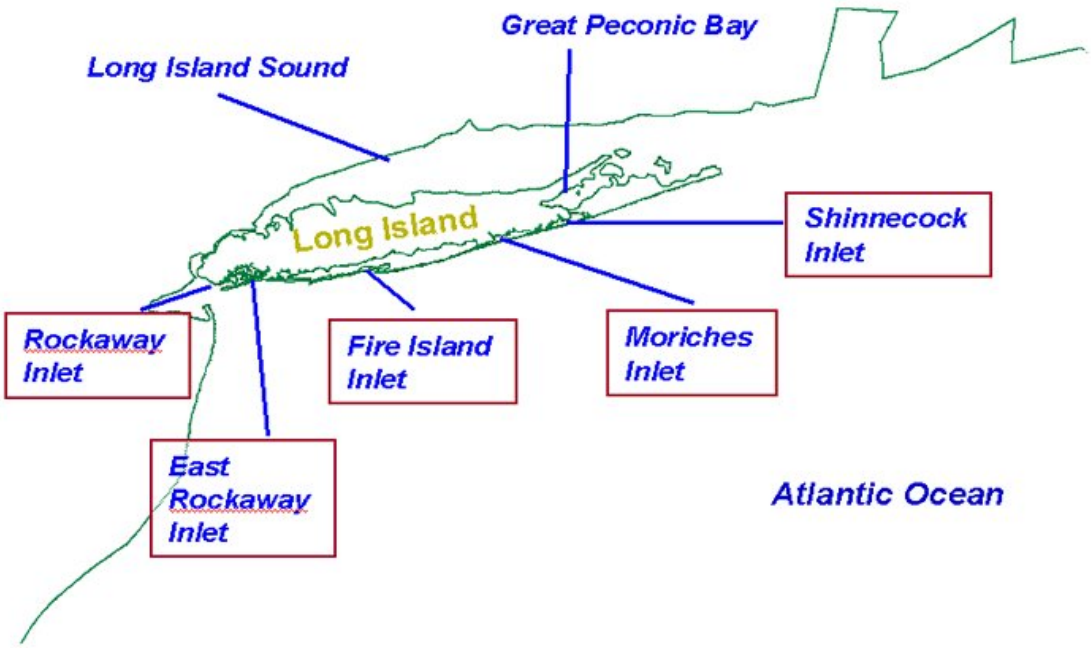

Figure 15 Schematic of Shinnecock Inlet Location

The site provides a test of the following aspects of the code and mesh generator:

- Ability to mesh a complex coastline and bathymetry with a variable density mesh.
- Input data from scattered bathymetric data points.
- Inclusion of tidal forcing from the Le Provost database.

Input files

Data files of bathymetry and coastline are available for this site from the ADCIRC website. The bathymetric data is in X/Y/Z format. We show a plot of the bathymetry in Figure 16.

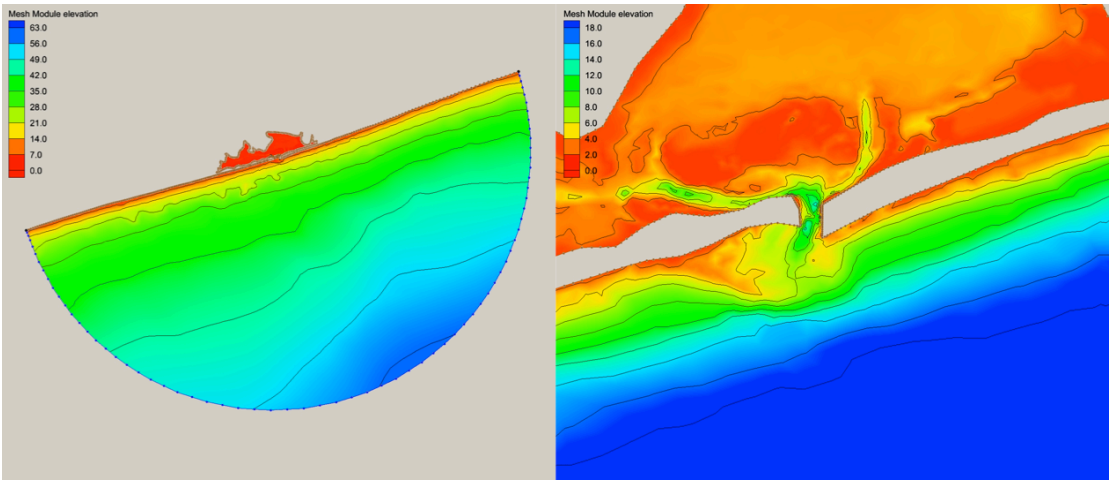

Figure 16 Bathymetry of Shinnecock Inlet. Left shows the bathymetry in the whole domain. Right shows the detailed bathymetry around the inlet

Mesh

We generate a mesh so that resolution is higher around the inlet where we expect faster currents and more complicated flow behaviour. The mesh is shown in Figure 17.

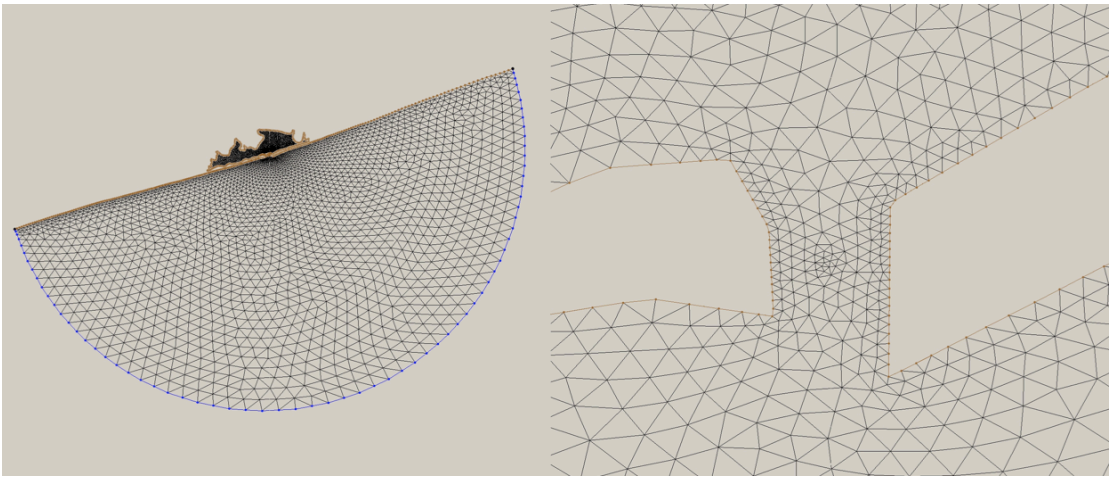

Figure 17 Grid used in model of Shinnecock Inlet. Left shows the whole mesh. Right the detailed mesh around the inlet.

Figure 18 shows the mesh projected onto Google Earth image, so as to give a better sense of the scale of the mesh. Note that due to the different projection the shape of the mesh appears different to that in Figure 17.

Figure 18 The mesh shown projected onto aerial photographs taken from Google Earth

Model configuration

Table 2 lists the key parameters set in DG ADCIRC for the Shinnecok Inlet case. The parameter values are based on values typically used in tidal modelling rather than any attempt to match local conditions as no data was available for this location. The purpose of this exercise was to demonstrate that the code may be applied to a realistic site, rather than provide a validation of shallow water

solvers for coastal applications. For modelling the sites which are being investigated in the work package it will, of course, be important to tune these parameters so that the model matches field measurements.

Parameter	Value	Notes
Time-step	1 s	Based on the CFL condition appropriate to the order of polynomial used (Kubatko et al., 2008)
Friction coefficient	0.005	For water depths < 2 m a higher friction coefficient is used based on Manning's formulation.
Eddy viscosity	$3.0 m^2 s^{-1}$	
Coriolis coefficient	0.0001	
DG polynomial order	2	
Numerical method	4^{th} order Runge-Kutta	Based on the requirement for this polynomial order given in Kubatko et al. (2008).

Table 2 Parameters used in Shinnecock Inlet model

The forcing conditions are derived from the Le Provost database of tidal amplitudes and phases. These are interpolated onto the boundary nodes. In this example, we use tidal constituents given by M2, S2, K1 and N2. These are dominated by the M2 tide which has a magnitude of 0.45~0.55m at the offshore boundary.

We start the model on 1 January 2000. The boundary values are linearly ramped over a period of 0.75 days at the start of the simulation.

Results

Typical results are shown below. Figure 19 shows how the tidal amplitude varies across the domain near to high tide. The phase difference across the width of the domain can be seen (the magnitude of the M2 constituent has a small spatial variation, so the difference in free surface is driven by the phase).

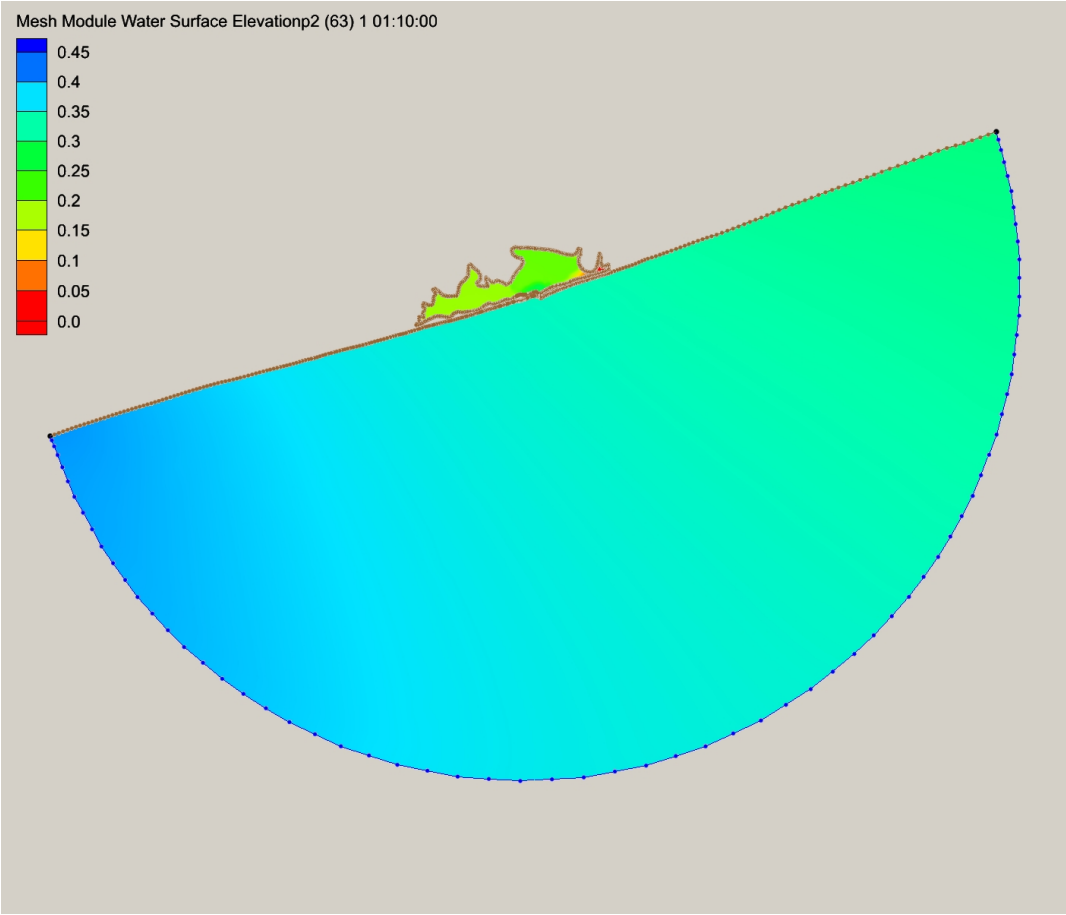

Figure 19 Variation in free surface close to high tide at Shinnecock inlet. Amplitude is in m.

We now examine the dynamics around the inlet in greater detail. Figure 20 shows the free surface elevation and current velocity across the inlet as the water ebbs out of the inlet. As the current magnitude is difficult to visualize from the current vectors on Figure 20, we show this more clearly in Figure 21. The model predicts that the flow is directed around the very shallow water immediately inland of the inlet as expected. We also observe that the model predicts an eddy structure at the outlet on the eastern side. These results appear to be realistic although we do not have field data for comparison.

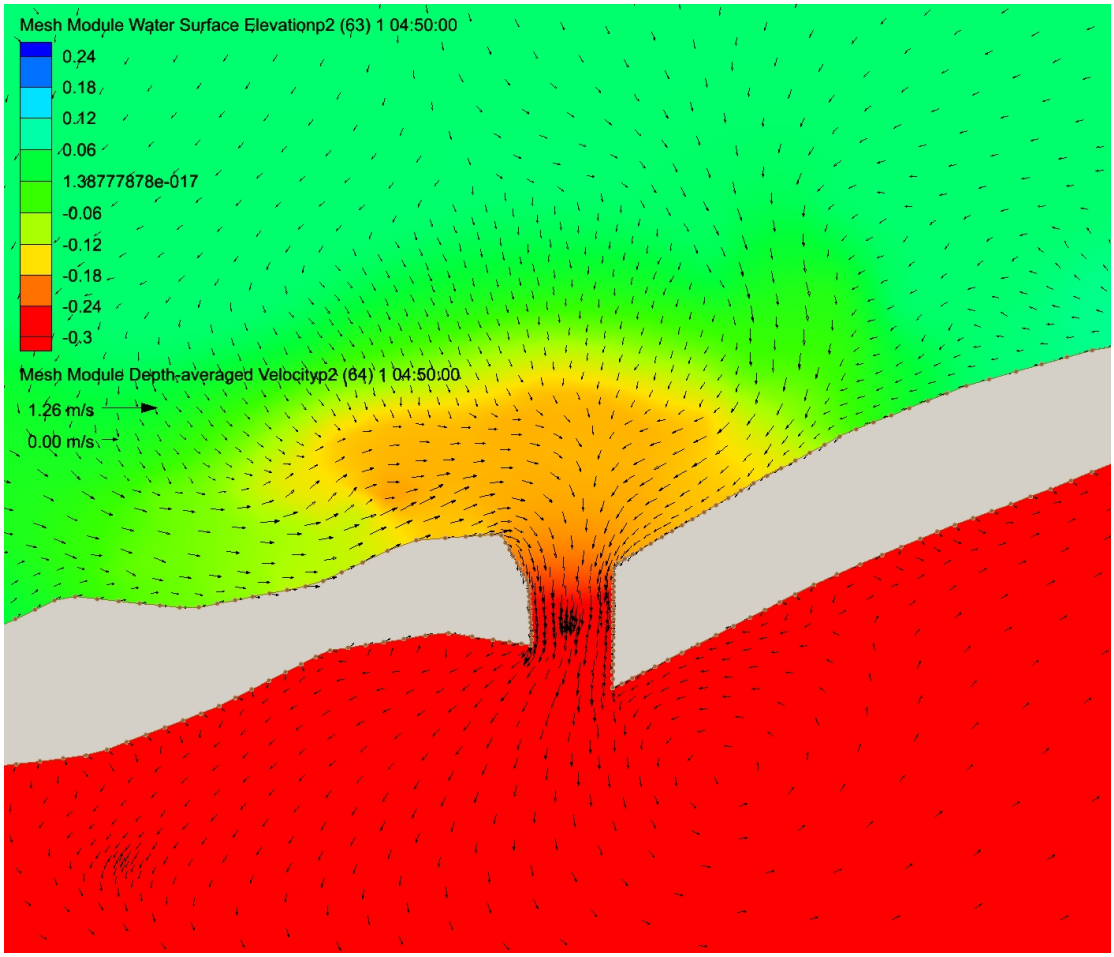

Figure 20 Free surface (shading) and current (arrows) for an ebb tide. Amplitude is in m.

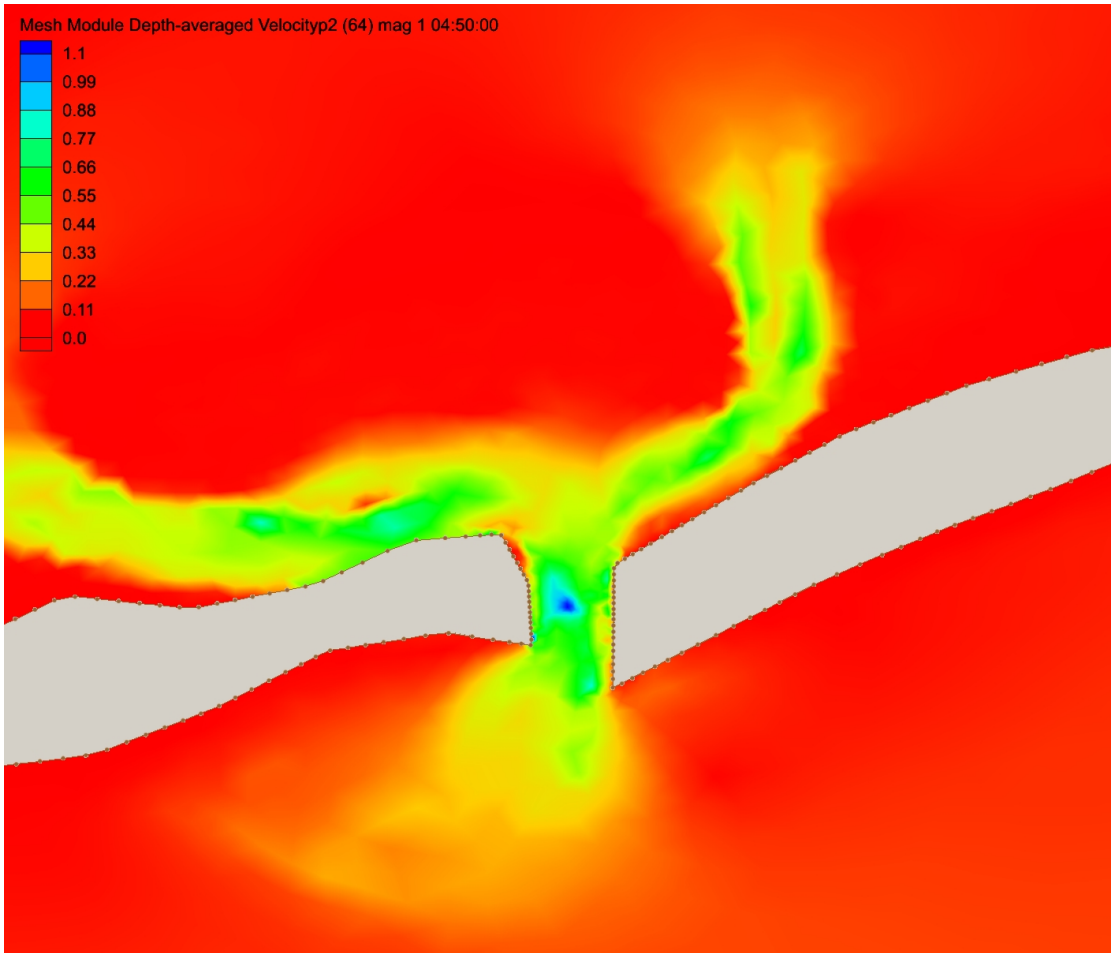

Figure 21 Magnitude of current during ebb. Magnitude is in m/s.

4. Applications

Shallow water numerical codes such as ADCIRC may be applied to a variety of problems in addition to the modelling of tides. The shallow water equations are applicable to waves for which $kh < \pi/10$ (Dean & Dalrymple, 1984). Examples are:

Storm surge

Storm surges are primarily caused by the wind stresses on the free surface of the water and the reduction in atmospheric pressure often associated with a storm. The relevant importance of these depends on the length of the storm and the speed at which the storm moves. In fast moving storms, such as hurricanes, pressure variations will dominate but for slow moving storms pressure changes need to be included in the model (Pugh, 1987). The wavelength of the storm

surge is typically of the order of hundreds of kilometers. Thus the vertical velocities will be small compared to the horizontal velocity component and the storm surge may be modelled using the shallow water equations. An example of such modelling carried out with ADCIRC is given by Westerink et al. (2008).

Wave set-up

To first order, wind generated waves do not transport mass. However, to second order there is transport of water associated with Stokes Drift. This becomes particularly important in shallow water. To balance the water transported by the waves a return current is generated that travels in the opposite direction to the wave, driven by the head created by the set-up near the shore. This is frequently coupled with the storm surge (Resio & Westerink, 2008) during violent storms.

The wave-set up may be modelled using a shallow water flow solver. Typically, this is driven by a wind/wave model and the two are coupled.

Oceanic currents

Oceanic currents are formed by the wind stress from the prevailing winds over a large expanse of ocean. Accurate modelling of oceanic currents may require representing variations of the flow with depth. However, the leading order characteristics may be given by a shallow water flow model.

Tsunamis

Tsunamis are generated by rapid displacement to the water mass. Most frequently these are due to tectonic movements but may also be due to other causes such as landslides. Tsunamis are long waves, and shallow water models accurately capture their propagation.

5. Sensitivities

Boundary conditions

Any numerical model is dependent on the boundary conditions that are used in it. Understanding the sensitivity of a model to the boundary conditions is crucial.

Offshore boundary condition

As part of this work package, this topic has been extensively explored. This material is being submitted to the European Wave and Tidal Energy Conference in Southampton (Adcock et al., 2011). This paper is self-contained and is presented as an appendix to this work package.

Bathymetry

An accurate bathymetric data set is vital to modelling tidal basin dynamics. The gradient of the bathymetry term is used in shallow water equations and thus any error or noise in the bathymetry will be exaggerated in the tidal model.

The quality of the bathymetry is particularly critical for modelling the energy extraction from basins. Small errors in bathymetry lead to relatively large errors in the estimate of bed friction coefficient (Draper, 2010). The amount of tidal energy in a basin is finite and the amount that may be extracted will always be a balance between that which is lost through friction, and that extracted by the turbines. Thus an accurate estimate of the bed friction, and in turn bathymetry, is vital for an accurate estimate of the energy which may be extracted from a basin.

Discretisation

Use of a numerical solution requires discretisation in both time and space. To give acceptable results these must be sufficiently resolved so as to accurately represent the solution. In a DG code spatial discretisation is related to the order of the elements, with higher order elements generally allowing a much coarser grid. In the numerical models being developed in this project grid convergence studies will be carried out to ensure that sufficient discretisation and that the results are not grid dependent.

6. Limitations

The limitations of the numerical model may be considered in two parts: the limitations of underlying equations, and the limitations of DG ADCIRC representation of them. We also consider the basin scale aspects that are not being considered in this work package.

Limitations of the shallow water equations for tidal modelling

A specification of this project is that the depth-averaged shallow water equations are used to model the tidal basin hydrodynamics. The shallow water equations provide an acceptably accurate model for most marine turbine locations. It is not generally possible to quantify the error due to the depth-averaged assumption other than for idealised situations (for instance an analytical error is calculated by Faltinsen and Timokha (2002) for the shallow water sloshing problem). The error will vary from site to site. Investigating this is not the primary purpose of this project. However, for each of the chosen sites it should be possible to determine whether the two-dimensional model is sufficiently accurate for engineering purposes. This will be based on our understanding of the tidal dynamics of the site and comparison between the numerical model and field measurements.

Bathymetric constraints

A fundamental limitation of a depth-averaged model is that a vertical current profile must be assumed and that the pressure is hydrostatic. Typically, the assumed vertical current profile will be log profile (Stansby, 2005), a $1/7^{th}$ power law across the whole depth, or a power law over the bottom half of the fluid and a constant in the top half (Soulsby, 1997). These profiles all have a similar form and once integrated over water depth give similar results in a depth-averaged model. These effects are essentially represented by the calibrated model parameters such as bed friction and eddy viscosity. There are examples where the real velocity profiles differ significantly from the forms suggested above. An example would be where flow passes over a sudden step in bathymetry and causes the flow to separate (similar to the eddy viscosity test above only with a vertical rather than horizontal step).

Another example that has been extensively studied experimentally is the flow around a conical island with shallow sloping sides (Chen & Jirka, 1995; Lloyd & Stansby, 2004). The flow pattern created by such geometry is highly complicated with both horizontal and vertical eddy structure. This complexity may lead to the velocity near the seabed being opposite in direction to that near the surface – in this situation the bed friction and eddy viscosity term will not be

evaluated realistically. As pointed out in Stansby (2005), this difficulty will occur in any depth-averaged model. Using a 2+1D model, where the profile is allowed to vary but is not fully resolved, or a full 3D model may give improved results although this still requires significant tuning. Whilst Stansby has shown that this tuning is possible for matching experiments where there are spatially dense measurements to calibrate the model, this level of data will be very expensive to collect for real locations. In the model of Shinnecock Inlet undertaken in this work it is likely that the eddy structure at the outlet is three-dimensional, given the bathymetry and the magnitude of the current. Hence the model may give poor results in the area where the eddy is predicted.

Of the sites that are to be studied in this work separate vertical and horizontal eddies are most likely to occur off Anglesey (Davies & Gerritsen, 2002).

Density

Areas where there are large vertical density variations will be poorly modelled by a (single layer) shallow water numerical scheme, as these density variations are not modelled. Flows of differing density are most frequently encountered in estuaries where there is an inflow of freshwater which mixes slowly with sea water. Another example, which combines both a high density and a rapid change in bathymetry, is the modelling of tides near certain ocean trenches. An instance of this is the Norwegian trench in the North Sea, where depth averaged models give poor results. Gross features, such as overall discharge and tidal amplitude may be insensitive to resolving density gradients. However, fine details, including tidal currents, are sensitive to density (Blumberg, 1976).

Use of a 3D model will improve accuracy but at considerable computational cost. Satisfactory results have also been found using a two layer shallow water flow solver (Lee et al., 2011).

Although, density variation influences the hydrodynamics of the Bristol Channel (Hamilton, 1973), these will not be accounted for in the present project. However, numerous studies using a depth-averaged approach have given satisfactory results for this location.

Energy extraction model

The present work involves a turbine model based on linear momentum actuator disc theory (LMADT) developed by Houlsby et al. (2008). This is a theoretical model for the energy extraction and headloss. Whilst this is a useful model, real turbines behave differently to that predicted by LMADT. It is an open question how good parameterising turbines using blockage ratio, Froude number and wake induction factor, is at capturing the characteristics of real turbines.

Limitations of DG ADCIRC numerical model

Many of the limitations of the discontinuous Galerkin ADCIRC code are common to all numerical models. A numerical model, by its nature, provides an approximate solution to the governing mathematical equations. However, from a practical engineering point of view, a numerical solution should be sufficiently accurate provided sensible grid convergence and stability checks are undertaken (Roache, 1998).

The most important practical limitation is the computational demands of the modelling. As set out in the EWTEC paper attached as an appendix, a sizeable area of ocean must be modelled to obtain accurate results. Thus, as set out in the previous deliverable, it is important to use a numerical code that is parallelised. Nevertheless, computation times will limit the number of numerical runs which may be made. This is limiting factor for all numerical models.

Other aspects not accounted for in the present work

Oceanography

The scope of this project is only to consider the tidal currents. Around the British Isles the tidal current is usually dominant. However, other currents are present, which are listed in the Applications section. As the power take off is non-linear these currents will, on average, enhance the power available. However, the authors believe most of these currents are intermittent at the sites considered in this work package and so this will only have a small effect on the average power take off. The importance of non-tidal currents can be quantified by considering the remaining flow after the current due to tidal constituents are subtracted.

This will be examined in WG3 WP3 where the detailed characteristics of the sites are discussed.

Devices will need to be designed for higher currents than we find in this work. For instance, based on the experience of past studies, for the Pentland Firth the 100 year storm surge is likely to be 1~2 m/s, which, if it coincides with a spring tide, would lead to a current of more than 6 m/s and a Froude number of more than 0.25. This would obviously greatly increase the loading on a tidal turbine or necessitate a design which can shut-down energy extraction when a high current is expected.

One positive aspect often discussed in connection with a tidal barrage is its potential role in protecting against coastal flooding from storm surge. Whilst the positive effect would be smaller, there would also be a benefit in reducing coastal flooding by introducing tidal turbines. These would provide extra friction and help to dissipate the storm surge. However, tidal turbines would be expected to marginally worsen any river flooding as the friction would reduce the outflow of water (this would not be a problem for a well designed barrage). It is worth noting that the Thames Barrier is closed more frequently because of fluvial flooding than for coastal flooding (Lavey & Donovan, 2005). Thus, it will be important to understand the effect on storm surge and fluvial flooding if tidal turbines are to be deployed on a large scale.

Wave climate

The change to the wave climate is likely to be small compared to the change in current, but may be significant. Tidal turbines will act similarly to a submerged permeable breakwater with high porosity. The most significant change will be caused if the breakwater induces wave breaking. If tidal turbines are deployed on a large scale in the Bristol Channel these will need to be accounted for in wave forecasting and hindcasting models in this region.

Morphological changes

The seabed is continually changing in form, both in terms of the timescale of an individual tide or storm but also over longer periods. The morphological changes are driven by sediment transport due to waves and currents.

Changes to sediment transport will take place at two scales. One is due to the local flow through and by-passing the turbine causing scour around the turbines. This may be considerable depending on the seabed conditions. There will also be changes to the sediment dynamics at the basin scale as the magnitude of the currents are modified. For the sites considered in this study this is most likely to be problematic in the Bristol Channel where there is a high degree of sediment mobility (Kirby & Parker, 1983). On the other hand, the Pentland Firth has such high currents that, at least in the Firth itself, very little sediment settles. Thus smaller morphological changes would be expected at this location.

Pollutant dispersal

Tidal currents play an important role in dispersing pollutants. Altering the currents will modify this dispersal. Preliminary studies of the changes to the motion of individual particles caused by tidal turbines have been carried out by Draper (2011) for idealised locations.

7. Conclusions

In this deliverable we have demonstrated that DG ADCIRC accurately solves the shallow water equations. Numerical tests have verified that the individual terms are correctly included in this model. Further we have shown that the code may be applied to a realistic location with complex coastline and bathymetry.

A discussion has been presented of the applications, limitations and sensitivities of the model. There are various aspects which will be important in designing tidal turbine farms that are not being examined in this work. There are also complexities in the physics of tidal basins which the model we are using cannot capture. However, it is expected that the modelling work being carried out in this project will give satisfactory results for both the power take off and the large scale changes to the hydrodynamics in the basin.

References

Adcock, T.A.A., Borthwick, A.G.L. and Houlsby, G.T. 2011 The Open Boundary Problem in Tidal Basin Modelling with Energy Extraction. Submitted to EWTEC 2011.

Armaly, B.F., Durst, F., Pereira, J.C.F., and Schonung, B. 1983 Experimental and theoretical investigation of backward-facing step flow. Journal of Fluid Mechanics, 127 473-496.

Bermudez, A., and Vazquez, M.E. 1994 Upwind methods for hyperbolic conservation laws with source terms. Computer Fluids, 423 8, 1049-1071.

Blumberg, A. F. 1976 The Influence of Density Variations on Estuarine Tides and Circulations. Esturine and Costal Marine Science. 6 209-215.

Brufau, P., Vazquez-Cendon, M.E., and Garcia-Navarro, P. 2002 A numerical model for the flooding and drying of irregular domains, International Journal for Numerical Methods in Fluids, 39, 247-275

Bunya, S., Kubatko, E.J., Westerink, J.J., and Dawson, C. 2009 A wetting and drying treatment for the Runge-Kutta discontinuous Galerkin solution to the shallow water equations. Comput. Methods Appl. Mech. Engrg., 2009, 198, 1548-1562

Chen, D., and Jirka, G. H. 1995 Experimental study of plane turbulent wakes in a shallow water layer. Fluid Dyn. Res., 16, 11–41.

Davies, A. M. and Gerritsen, H. 1994 An intercomparison of three-dimensional tidal hydrodynamic models of the Irish Sea. Tellus A, 46: 200–221

Dean, G. D. and Dalrymple, R. A. 1984 Water Wave mechanics for engineers and scientists. Advanced series on Ocean Engineering. Volume 2. World Scientific.

Denham, M.K., and Patrick, M.A. 1974 Laminar flow over a downstream-facing step in a two-dimensional flow channel. Chemical Engineering Research and Design, 52a, 361-367.

Draper, S. 2010 Notes on the non-uniqueness of depth-averaged velocity. Unpublished.

Draper, S. 2011 Some Analytical and Numerical Studies of Tidal Stream Energy Extraction in Coastal Basins. DPhil thesis. University of Oxford

Draper, S., Houlsby, G.T., Oldfield, M.L.G., Borthwick, A.G.L 2010 Modelling tidal energy extraction in a depth-averaged coastal domain. Renewable Power Generation, IET , 4(6), 545-554

Ern, A., Piperno, S., and Djadel, K. 2008 A well-balanced Runge-Kutta discontinuous Galerkin method for the shallow-water equations with flooding and drying. International Journal for Numerical Methods in Fluids, 58, 1-25.

Eskilsson, C., and Sherwin, S.J. 2000 A triangular spectral/hp discontinuous Galerkin method for modelling 2D shallow water equations. International Journal for Numerical Methods in Fluids 201; 1:1

Faltinsen, O. M. and Timokha, A. N. 2002 Asymptotic modal approximation of nonlinear resonant sloshing in a rectangular tank with small fluid depth. 470, 319-357

Giraldo, F.X., and Warburton, T. 2008 A high-order triangular discontinuous Galerkin oceanic shallow water model. International Journal for Numerical Methods in Fluids 56, 899-925

Houlsby, G.T., Draper, S. & Oldfield, M.L.G. 2008 Application of linear momentum actuator disc theory to open channel flow. Technical Report OUEL 2296/08, University of Oxford

Lavery, S. & Donovan, B. 2005 Flood risk management in the Thames Estuary looking ahead 100 years. Phil. Trans. R. Soc. A 363 (1831) 1455-1474

Kirby, R. and Parker, W. R. 1983 Distribution and Behavior of Fine Sediment in the Severn Estuary and Inner Bristol Channel, U.K. Canadian Journal of Fisheries and Aquatic Sciences. 40 83-95

Kubatko, E. J. Dawson, C. and Westerlink, J.J. 2008 Time step restrictions for Runge–Kutta discontinuous Galerkin methods on triangular grids. J. Comp. Phys. 227(23) 9667-9710

Kubatko, E. J., Westerink, J. J., and Dawson, C., 2006 hp Discontinuous Galerkin methods for advection dominated problems in shallow water flow, Comput. Methods Appl. Mech. Engrg. 196 437-451

Lee, W-K., Borthwick, A. G. L. and Taylor, P. H. 2011 A fast adaptive quadtree scheme for a two-layer shallow water model. Journal of Computational Physics. 230(12) 4848-4870.

Lloyd, P. M., and Stansby, P. K. 1997 Shallow-water flow around model conical islands of small side slope. I: Surface-piercing. J. Hydraul. Eng., 123(12), 1057–1067.

Hamilton, P. 1972 The Circulation of the Bristol Channel. Geophys. J. R. Astr. Soc. 32 409-422

Militello, A and Zundel, A. K. 2002 Coupling of Regional and Local Curculation Models ADCIRC and M2D. Technical report, US Army Corps of Engineers ERDC/CHL CHETN-IV-42

O'Leary, R.A., and Mueller, T.J. 1969 Correlation of physical and numerical experiments for incompressible laminar separated flows. Technical Report, Notre Dame University Ind. Coll. of Engineering

Pugh D.T. 1987 Tides, Surges, and Mean Sea-Level, Chichester: John Wiley & Sons

Resio, D. T. and Westerink J. J. 2008 Modeling the physics of storm surges. Physics Today 61(9), 33-39

Roache, P. J. 1988 Verification and Validation in Computational Science and Engineering. Hermosa Publishers, Albuquerque, New Mexico

Schlichting, H. 1986 Boundary Layer Theory. McGraw-Hill, New York

Soulsby, R. 1997 Dynamics of Marine Sands. Thomas Telford

Stansby, P. K. 2006 Limitations of Depth-Averaged Modeling for Shallow Wakes. J. Hydr. Engrg. 132, 737-740

Sutherland, G., Foreman, M. and Garrett, C. 2007. Tidal current energy assessment for Johnstone Strait, Vancouver Island. J. Power and Energy, 221, 147-157

Westerink, J. J., and Coauthors, 2008 A Basin to Channel-Scale Unstructured Grid Hurricane Storm Surge Model Applied to Southern Louisiana. Mon. Wea. Rev., 136, 833–864

Wijbenga, J. H. A. 1985 Determination of flow patterns in rivers with curvilinear coordinates. Prox 21st IAHR Congr. Melbourne.